

7.4 Analysis Verification Testing

The analysis verification tests provide data that define the accuracy of the damage tolerance analysis tools relative to their ability to predict the crack growth behavior of the structure under operational conditions. In essence, these tests are conducted to verify individual or collective elements of the damage integration package that will be used to conduct damage tolerant life analysis studies. Analysis verification tests include those tests that are used to verify stress-intensity factor calculations, residual strength methods, crack growth calculations, and test spectrum truncation procedures. The tests range in difficulty from constant amplitude tests on fairly simple structural geometries to flight-by-flight load type tests conducted on structures that simulate isolated design features contained in full-scale structural components. These tests are typically conducted during the design analysis and development testing phase of the contract prior to testing the full-scale structure and major components. Additional testing may also be necessary subsequent to the results of the full-scale flight and ground tests to support interpretation and evaluation of cracking problems.

7.4.1 Structural Parameter Verification Techniques

The current analytical procedures for developing the stress-intensity factor (K) associated with two-dimensional structural geometries have been extensively verified. The verification of the tools required to solve three-dimensional structural geometry problems, however, is still receiving major attention. This subsection reviews the experimental techniques utilized to verify the analytical procedures for obtaining stress-intensity factors for two- and three-dimensional geometries.

For the two-dimensional crack geometries, the engineer has the opportunity to employ four different types of experimental tests to verify the stress-intensity factor solution for the given problem: compliance (displacement/load) measurements [Bubsey, et al., 1973], moiré fringe techniques [Kiu & Ke, 1975], photoelastic procedures [Kobayashi, 1973], and crack growth rate testing [James & Anderson, 1969]. In the realm of the three-dimensional problem, only two of the above tests can be relied upon: photoelastic procedures [Smith, 1975], and crack growth rate testing [Grandt & Sinclair, 1972; Grandt & Hinnerichs, 1974].

7.4.1.1 Compliance

The compliance measurement test is based on the relationship between compliance (C), which is a measure of stored energy in the structure, and the strain energy release rate (G). The relationship as discussed in Section 1.3 is:

$$G = \left(\frac{P^2}{2B} \right) \left(\frac{\partial C}{\partial a} \right) \quad (7.4.1)$$

where P is the applied load, B is the structural thickness, and a is a measure of crack length. The compliance in Equation 7.4.1 is associated with the displacement of the load points along the axis of loading. It should be noted that displacements not along the axis of loading cannot be used in the calculation of the strain energy release rate (G). Once the relationship between G and C has been established the stress-intensity factor (K) is calculated using:

$$K = \sqrt{GE'} \quad (7.4.2)$$

where $E' = E$, the elastic modulus, for plane stress problems and $E' = E/(1-\nu^2)$ for plane strain problems, ν is Poisson's ratio. Since the bulk of the material in any given structure is subject to plane stress conditions, the better correlations are obtained between analytically determined K solutions and compliance determined K solutions based on the plane stress formulation of Equation 7.4.2.

7.4.1.2 Moiré Fringe

The moiré fringe technique for obtaining the stress-intensity factor for a through-thickness crack (two-dimensional geometry) is based on the measurement of in-plane displacements (or strains) in the crack tip region. The moiré fringes, which leads to displacement or strain measurements, are developed as a result of an interference created by an optical mismatch of two grid patterns; one pattern is the model grid which is placed on the structure, the other is the reference grid which has the same pattern as the model grid in the unloaded condition. As the moiré fringes are converted to, say, displacement measurements in the crack tip region, the displacement (δ) of the crack surfaces close to the crack tip is related to the stress-intensity factor (K) through the relation (plane stress-linear elasticity assumed)

$$\delta = \frac{8K}{E} \left(\frac{r}{2\pi} \right)^{1/2} \quad (7.4.3)$$

where E is the elastic modulus and r is the distance from the crack tip. Typically, measurements are made of the displacement as a function of distance from the crack tip; and, the collection of these results are used with a linear regression equation to estimate the value of K .

Continuing evolution of the moiré interferometry techniques have produced methods for increased displacement sensitivity which are covered by a review paper by Post, et al. [2000] In a method called microscopic moiré interferometry, two techniques have evolved which are used sequentially: a) an immersion interferometer uses a fluid coupling media to produce virtual reference gratings of 4800 lines/mm – double the usual basic sensitivity, b) a complementary technique uses optical/digital fringe multiplication by fringe shifting, along with an efficient algorithm to generate an enhanced contour map of the displacement field. The two advances work in concert to result in an overall sensitivity multiplier as high as 24X.

Even planar surfaces are no longer a strict requirement for using moiré. Work by Boeman [1991] and later expanded by Mollenhauer [1997] have developed innovative methods for imaging the inner surfaces of bolt holes in composite plates.

Other variations include shadow moiré, which is useful for higher in-plane displacements, again as with regular moiré, increased sensitivities can be obtained using the optical/digital fringe multiplication techniques.

In work by Epstein and Dadkah [1993], applications to fracture mechanics solutions have been pursued. Moiré interferometry measures the stress intensity factor local to the crack-tip without relying on compliance calculations, a savings in instrumentation complications for both fracture and corrosion studies. Portable field units have been developed at Idaho National Engineering Lab for extending the use to maintenance and field activities.

A comprehensive review of experimental mechanics techniques and applications is included in Rastogi [2000].

7.4.1.3 Photoelasticity

Photoelastic techniques are based on the bi-refrangent characteristics exhibited by transparent plastic materials of specific tailored compounds of plexiglas, polycarbonate, and epoxy resins. These plastics, under load, develop an isochromatic fringe pattern that can be directly related to the maximum shear stresses in the geometry being analyzed. The photoelastic materials can be selected to match with the expected elongation of the substrate material. In [Table 7.4.1](#), the photoelastic test materials are bracketed into three levels by expected elongation range. The maximum measurable strain for a particular photoelastic coating depends upon its stress-strain curve and the linearity of photoelastic behavior.

Table 7.4.1. Coating Selection for Elongation Levels

Coating Material	Maximum Elongation	Typical Application
PS-1	5%	Testing on metals, concrete, glass, and hard plastics in the elastic and elastoplastic ranges
PS-8	3%	
PL-1	3%	
PL-8	3%	
PS-3	30%	Testing on soft materials such as rubber, plastics and wood
PL-2	50%	
PL-3	>50%	
PS-4	>40%	
PS-6	>100%	Testing on soft materials such as rubber, plastics and wood

Chart courtesy of Vishay Measurements Group, Inc.

The bi-refrangent sensitivity is another important factor to consider when choosing a photoelastic coating [Vishay Measurements Group, Inc., 2001]. The overall sensitivity of the strain measurement system depends on:

- The sensitivity of the coating is expressed by the fringe value, ϕ . The fringe value represents the difference in principle strains, or the maximum shear strain, required to produce one fringe. The lower this parameter, the more sensitive the coating,
- The sensitivity of the polariscope system for examining the photoelastic pattern and determining the fringe order, N .

The primary difference between the approach used for two- and three-dimensional work is that two-dimensional models can be directly analyzed under load whereas the three-dimensional model must be reduced to a two-dimensional model before the crack tip fringe information can be recovered. To obtain the fringe results from the three-dimensional model, the isochromatic fringe pattern must first be frozen in place while the model is under load; the stress freezing is accomplished through a thermal treatment that takes the material above a critical temperature for a hold-time period which is followed by a slow cooling. Subsequent to the stress freezing operation, the three-dimensional model is sliced up to obtain a two-dimensional slice that

contains the crack segment of interest. This two-dimensional slice is then interrogated with normal photoelastic equipment (polariscope) to recover the imbedded fringe information.

A new development for building 3-D structural models is by using stereolithography (SLA). [TECH, Inc. 2001] SLA is a rapid prototyping process by which a product is created using an ultra-violet (UV) curable liquid resin polymer and advanced laser technology. Using a CAD package such as Pro/Engineer, SolidWorks, or other solid modeling software, a 3-D solid model is exported from the CAD package as an .stl file. The .stl file is then converted into thin layers. The sliced model, in layers, is then sent to the SLA machine. The SLA machine uses its laser to cure the shape of the 3-D CAD model on a platform in the vat of resin from the bottom up, one layer at a time. As each layer is cured, the platform is lowered the thickness of one layer so that when the part is completely built, it is entirely submerged in the vat. Stereolithography is capable of creating the most complex geometries quickly and precisely.

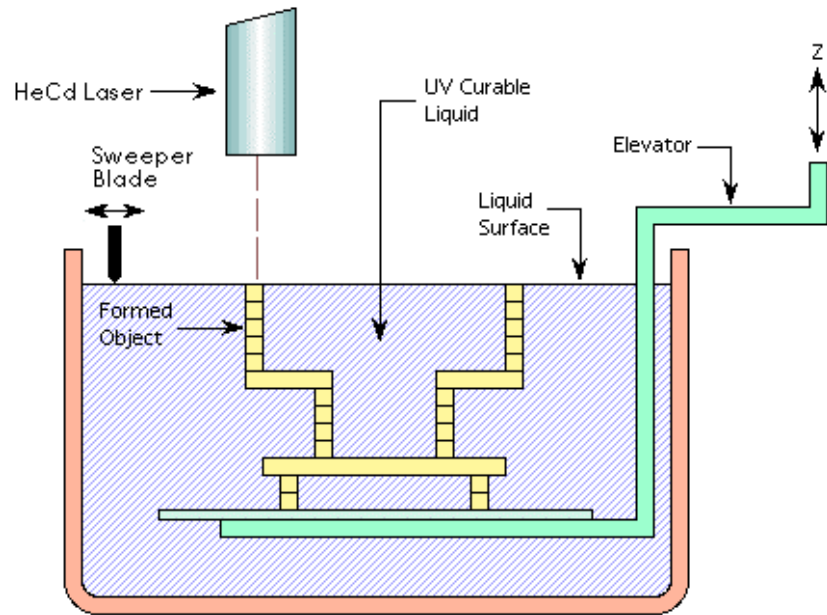


Figure 7.4.1. Stereolithography process diagram (Courtesy of TECH, Inc.)

The analysis of crack tip fringe information is the same for both the two- and three-dimensional models. For Mode I loading, the stress-intensity factor (K) is obtained using:

$$K = \sqrt{\pi r} \left(8\tau_{max}^2 - \sigma_0^2 \right)^{1/2} - \sigma_0 \quad (7.4.4)$$

where σ_0 is an unknown pseudo-boundary stress, r is the distance directly above the crack tip on an axis perpendicular to the crack path, and τ_{max} is the maximum shear stress obtained from the stress-optic law

$$\tau_{max} = \frac{nf}{2B} \quad (7.4.5)$$

with n the photoelastic fringe order, f the material fringe value, and B the thickness of the two-dimensional model or slice. The shear stress (τ_{max}) is typically analyzed using a truncated Taylor series that describes the behavior in the crack tip region, i.e.

$$\tau_{max} = \frac{A}{r^{0.5}} + \sum_{N=0}^M B_N r^{N/2} \quad (7.4.6)$$

where Smith [1975] suggests N is chosen to be the lowest possible number that results in Equation 7.4.6 providing a good fit to the shear stress data. [Figures 7.4.2](#) and [7.4.3](#) illustrate the two basic steps used in determining the stress-intensity factor from photoelastic experiments [Smith, 1975]. For both three-dimensional surface crack models considered, the thin two-dimensional slice that was analyzed for the crack-tip fringe pattern was taken through the point p . The slice was perpendicular to the crack plane and oriented so that the slice was through the thickness; thus the slice had the appearance of a single edge cracked geometry.

[Figure 7.4.2](#) describes the shear stress distribution (points) and the corresponding least-squares derived truncated Taylor series expansion (curve) for the two surface crack geometries considered. [Figure 7.4.3](#) illustrates how Equation 7.4.6 and 7.4.4 are combined to extrapolate the photoelastic data to the crack tip. [Figure 7.4.3](#) portrays the stress-intensity factor based on photoelastic data (K_{AP}) as the ratio of the photoelastic result to the preexisting theoretical result. Note that the photoelastic result is calculated from Equation 7.4.4 where the pseudo boundary stress (σ_o) is taken as zero. This stress is accounted for through the $N=0$ term of Equation 7.4.6. The curves in [Figure 7.4.3](#) are based on the truncated Taylor series solutions obtained from the data in [Figure 7.4.2](#). In both cases shown, the extrapolations lead to reasonable estimates of the theoretical results and are somewhat typical of what one might expect from photoelastic estimates of the stress-intensity factor.

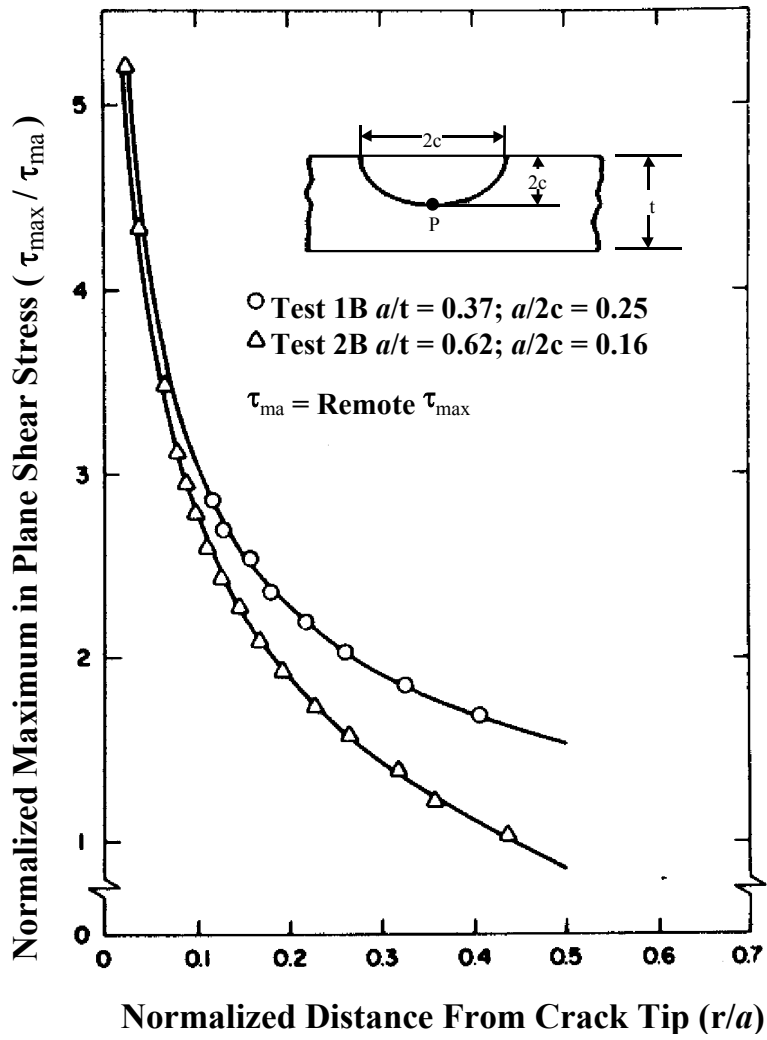


Figure 7.4.2. Typical Maximum Shear Stress Data Modeled with a Truncated Taylor Series Equation [Smith, 1975]

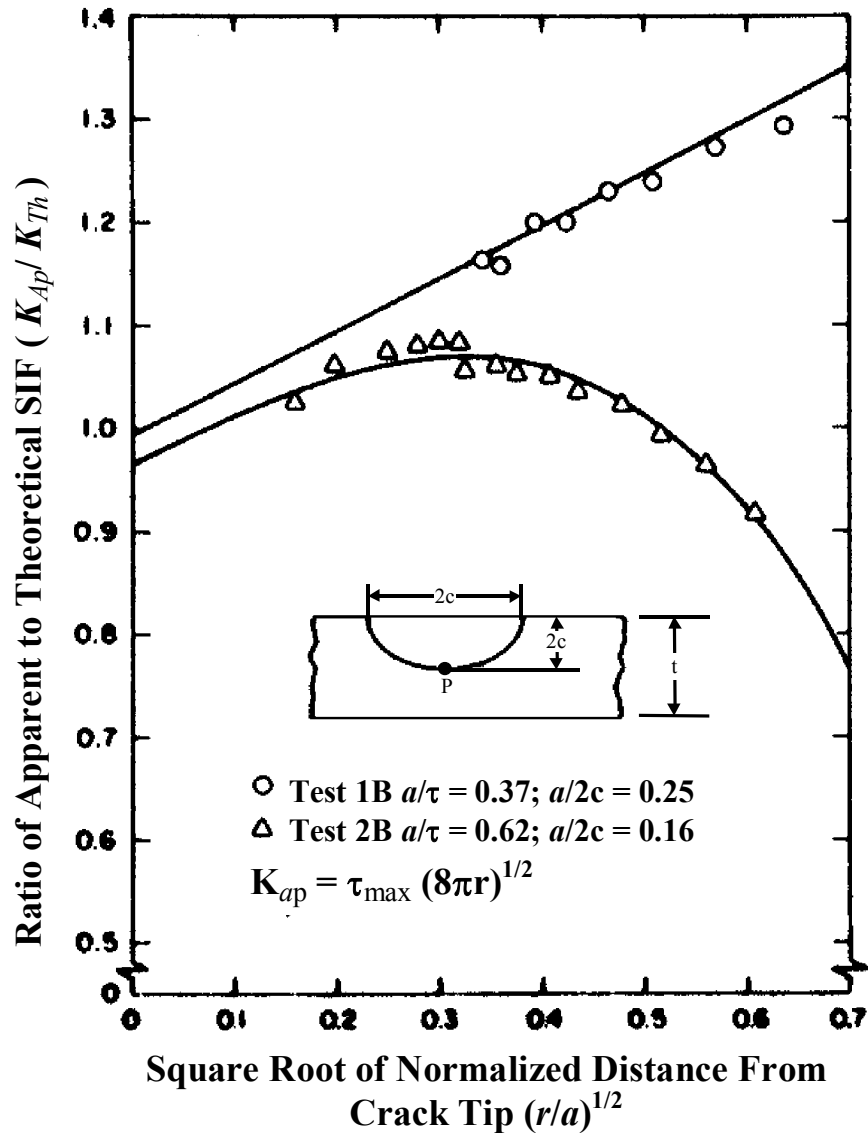


Figure 7.4.3. Extrapolation of Equation 7.4.4 Based on the Truncated Taylor Series Equation Results Presented in Figure 7.4.2 [Smith, 1975]

7.4.1.4 Crack Growth Rate

The basic hypothesis of the fracture mechanics approach to fatigue is that crack growth rate data can be described as a function of a stress-intensity factor (K) parameter associated with the fatigue loading. For constant amplitude loading, the parameter is the stress-intensity factor range (ΔK); and for steady-state variable amplitude loading histories, the parameter might be a root mean square value of the stress-intensity factor (K_{rms}). Once the basic hypothesis has been verified, crack growth data can be generated using relatively simple specimens; such data are independent of stress level, crack length, and structural test geometry, and thus can be related to the behavior of complicated structural geometries through the use of the stress-intensity factor.

The transferability of the crack growth rate data using the stress-intensity factor has provided a semi-inverse procedure for estimating the stress-intensity factor for complicated crack problems.

The semi-inverse procedure depends on the availability of two pieces of information:

- crack growth rate data for the structure for which the stress-intensity factor will be estimated, and
- crack growth rate versus stress-intensity factor type data collected for the material subjected to the same type of loading history to which the structural crack has been exposed.

The semi-inverse procedure relies on using the structure's crack growth rate (information item 1) to interpolate the material's crack growth rate/stress-intensity factor relationship (information item 2) to estimate the structure's stress-intensity factor. [Figure 7.4.4](#) provides a schematic illustrating how the two information items are used to obtain the structure's stress-intensity factor relationship.

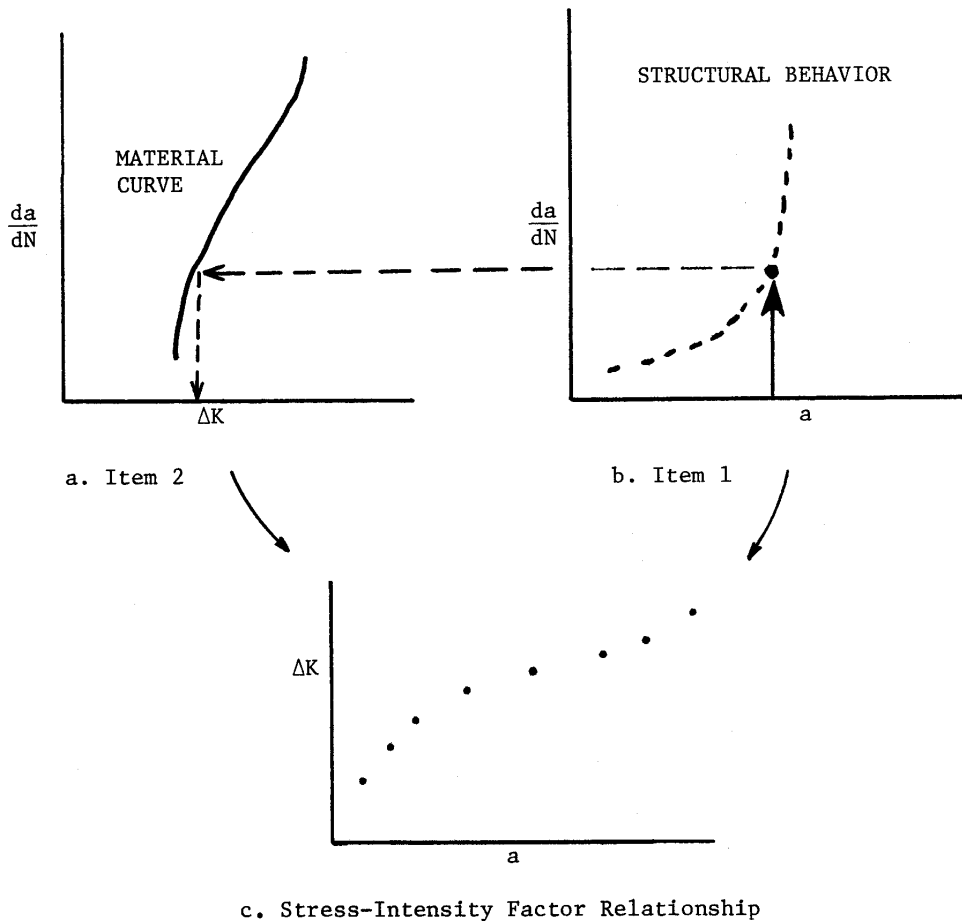
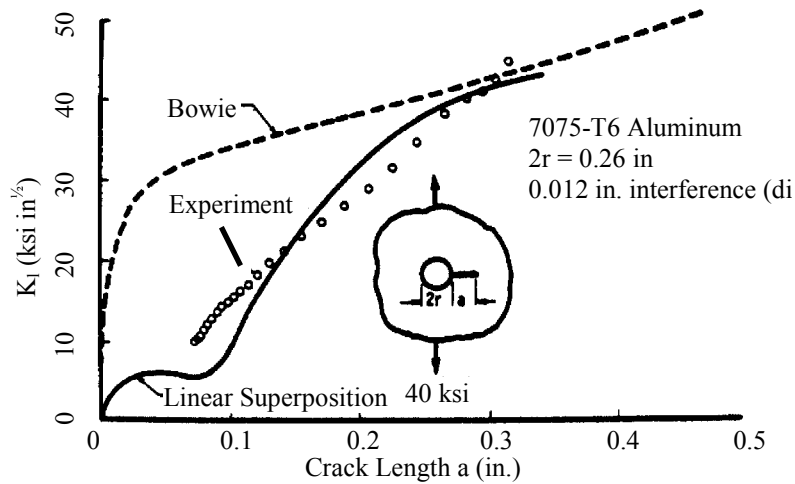
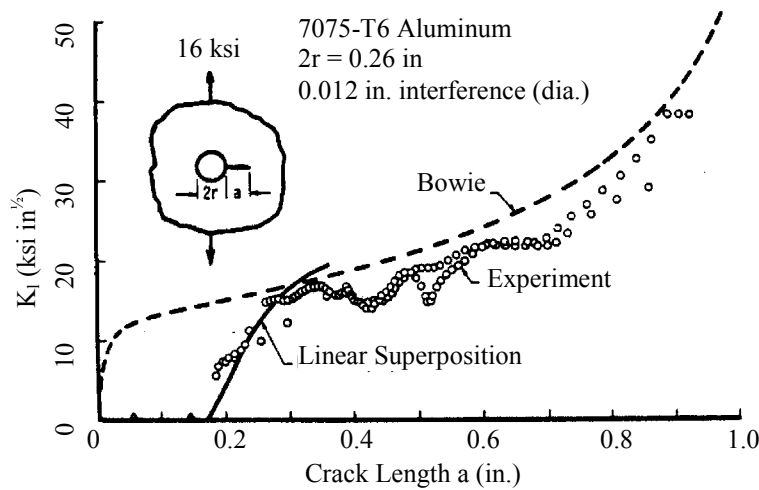


Figure 7.4.4. Semi-Inverse Fatigue Crack Growth Rate Determination of Stress-Intensity Factors

Grandt and coworkers [Grandt & Sinclair, 1972; Grandt & Hinnerichs, 1974] have applied the semi-inverse procedure to a number of problems of Air Force interest. [Figure 7.4.5](#) describes the results for a radially cracked cold-worked hole that was subjected to two different levels of remote loading. It can be seen from the figure that the stress-intensity factor values obtained from the semi-inverse procedure (the data points) describe a relatively smooth function and closely approximate the analytical results marked linear superposition. Due to the cold-working operation, the stress-intensity factor is also seen to be substantially below that associated with the open hole configuration (curve marked Bowie), which well demonstrates the benefit of cold working.



a. Remote Stress = 40 ksi, $R = 0$



a. Remote Stress = 16 ksi, $R = 0$

Figure 7.4.5. Stress-Intensity Calibration for a 0.26 Inch Diameter Hole Cold-worked to Achieve a 0.012 Inch Diametrical Interference in 7075-T6 Aluminum Alloy (0.25 Inch Thick)

7.4.2 Residual Strength Methods-Verification

In Section 4, the residual strength analysis was discussed which requires a material model describing the fracture process, the specific materials data that support the model for the structural thickness and loading conditions, and the ability to derive the value of the controlling structural parameter (such as the stress-intensity factor) for the cracked structure. There are a series of residual strength tests that can be conducted during the course of the design analysis and development test activity (JSSG-2006 paragraph 4.12.2) that will support the verification of residual strength analysis capability in aircraft safety-of-flight critical structure. For example, a manufacturer could choose to conduct some constant amplitude fatigue crack growth rate tests

using radial-corner-cracked-hole type specimens or part-through thickness cracked type specimens in order to verify the stress-intensity factor analysis part of the damage integration package. Instead of cycling such constant amplitude tests to failure, the tests could be stopped prematurely and the specimens pulled to fracture. By monitoring these fracture tests and recording critical events as a function of load, the manufacturer can build a database that can be utilized to verify the applicability of various material (fracture) models proposed for the residual strength analysis.

An example illustrating some of the initial steps in verifying the applicability of a new type of fracture model can be obtained from a review of the work of Wang and McCabe [1976]. One of the first steps in verifying any residual strength analysis is to demonstrate the transferability of the data between simple cracked geometries.

Wang and McCabe considered the applicability of the R-curve (K_R) analysis to the prediction of residual strength of aircraft structures. At the time of their study, there was almost no documentation that supported the transferability of R-curve data. Wang and McCabe employed two types of crack-line-wedge-loaded compact [C(W)] specimens to provide the basic materials data and then performed a residual strength analysis on middle-crack tension [M(T)] panels. They also directly compared the R-curves from the two cracked geometries; [Figure 7.4.6](#) describes one of their comparisons.

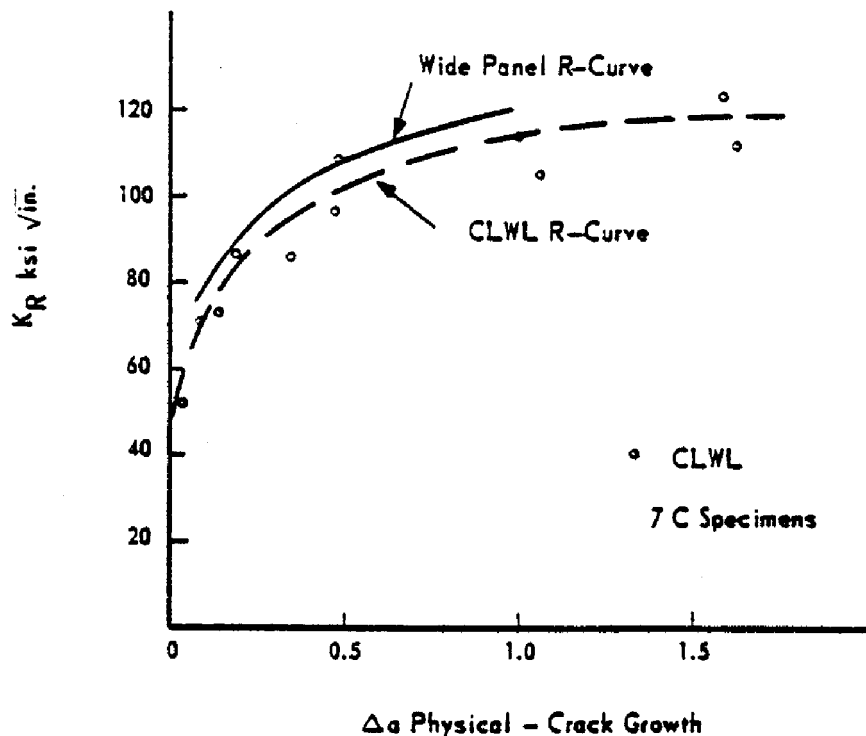


Figure 7.4.6. R-Curve Comparison for 7475-T61 Aluminum [Wang & McCabe 1976]

The Wang and McCabe residual strength results are summarized in [Table 7.4.2](#) and in [Figure 7.4.7](#). They were able to predict the gross stress at fracture, i.e. the residual strength, on the average to within 5 percent (on the conservative side) of the experimental results. Their most non-conservative prediction was only about 8 percent higher than the experimental value.

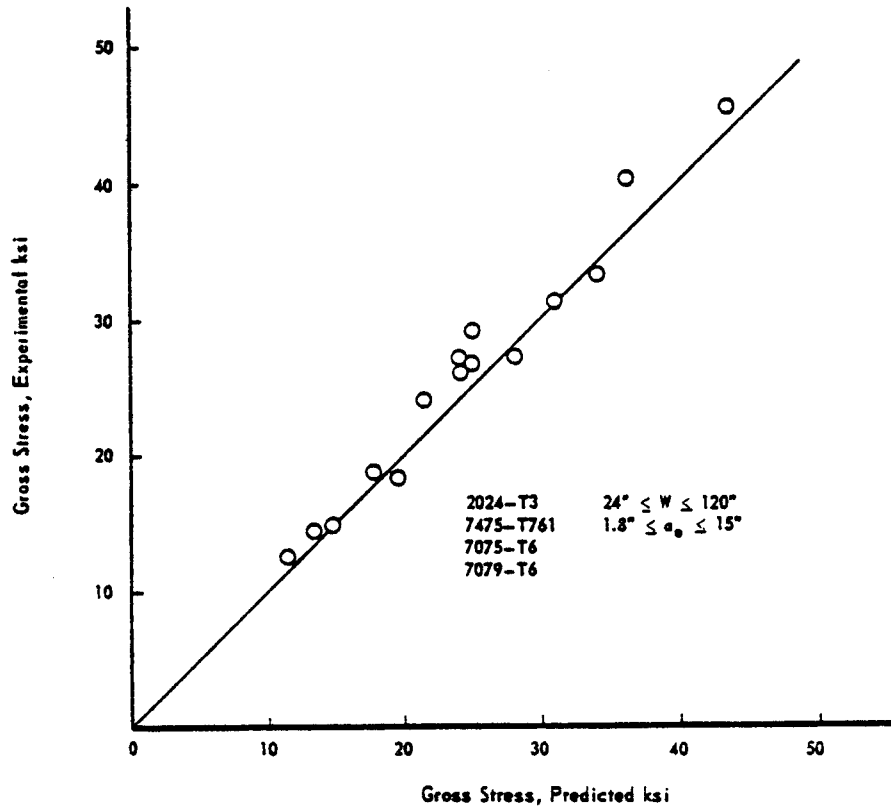


Figure 7.4.7. Summary of the Capability of the R-Curve Method for Predicting the Residual Strength of Center-Cracked Panels Using CLWL Specimen Data [Wang & McCabe 1976]

Table 7.4.2. Comparison Of CLWL Predicted Instability Conditions To Experimentally Determined Values In Middle-Cracked Panels.

			Half Crack Length (in)		Gross Stress, Fracture (ksi)		K _c ksi √in.		Net Section Stress, predicted ksi
Material	Width (in.)	a ₀ (in.)	Predict	Exper.	Predict	Exper.	Predict	Exper	
2024-T3	24	4.0	5.64	4.79	24.9	26.7	121.9	116	46.6
	36	5.4	7.43	7.03	24.1	26.1	130.5	134	40.8
	120	10.0	12.57	13.46	21.6	24.22	139.5	162	27.3
	120	15.0	17.66	19.05	17.8	18.7	140.1	156	25.2
7475-T761	36	1.8	2.91	2.65	43.5	45.2	133.8	133	51.8
	36	3.6	4.85	4.75	34.1	33.1	139.4	135	46.6
	36	5.4	6.70	6.50	28.1	27.2	141.1	134	44.8
	48	4.8	6.12	5.90	31.1	31.2	142.2	139	41.7
	120	10.0	11.46	11.05	23.8	27.2	146.1	164	29.3
	120	15.0	16.50	16.05	19.5	18.1	147.3	133	26.9
7075-T6	30	4.87	5.28	5.23	13.4	14.35	59.2	63	20.7
	48	7.0	7.42	7.3	11.5	12.5	59.0	63	16.6
7079-T6	48	7.0	7.49	8.05	14.9	14.95	77.0	78	21.6
7475-T61	36	1.8	2.54	2.65	35.9	39.8	102.6	118	41.8
	48	4.8	6.13	5.7	25.1	29.25	114.8	129	33.7
	120	10.0	11.67	-	19.3	-	119.7	-	24.0

The next step in verifying the residual strength prediction model is through the testing of built-up (multiple-load-path) type structure. Such structures have the attributes of transferring load during crack propagation as well as of possibly arresting the running crack before a catastrophic failure of the complete structure occurs. As discussed in Section 11, the development of an accurate value of the structural parameter K, the stress-intensity factor, requires that the structural analyst properly account for load transfer, joint deformations, fastener effects, etc. As such, the testing of built-up structures can result in the verification of the stress-intensity factor (or other appropriate parameter) estimates as well as the material failure model and its supporting data.

As an example of results obtained to validate the use of a residual strength model for built-up structure with fracture arrest features, consider the work of Swift and Wang [Swift, 1971; Swift & Wang, 1970]. They tested extremely large flat panels with longerons and frames. The longerons were either T or hat sections. The frames were attached to the skin with shear clips; in some cases, extra tear straps were used as crack stoppers. [Figure 7.4.8](#) describes a comparison of their predicted residual strength curves for four different configurations with the experimental results shown as points (initiation/arrest as appropriate). In most cases, the analysis was shown to be within 5 percent of predicting the experimental observation. Additional examples of residual strength verification tests for model transferability using single-load-path and built-up

structures can be found in Liu & Eckvall [1976], Verette, et al. [1973, 1977], Liebowitz [1974], and Potter [1982].

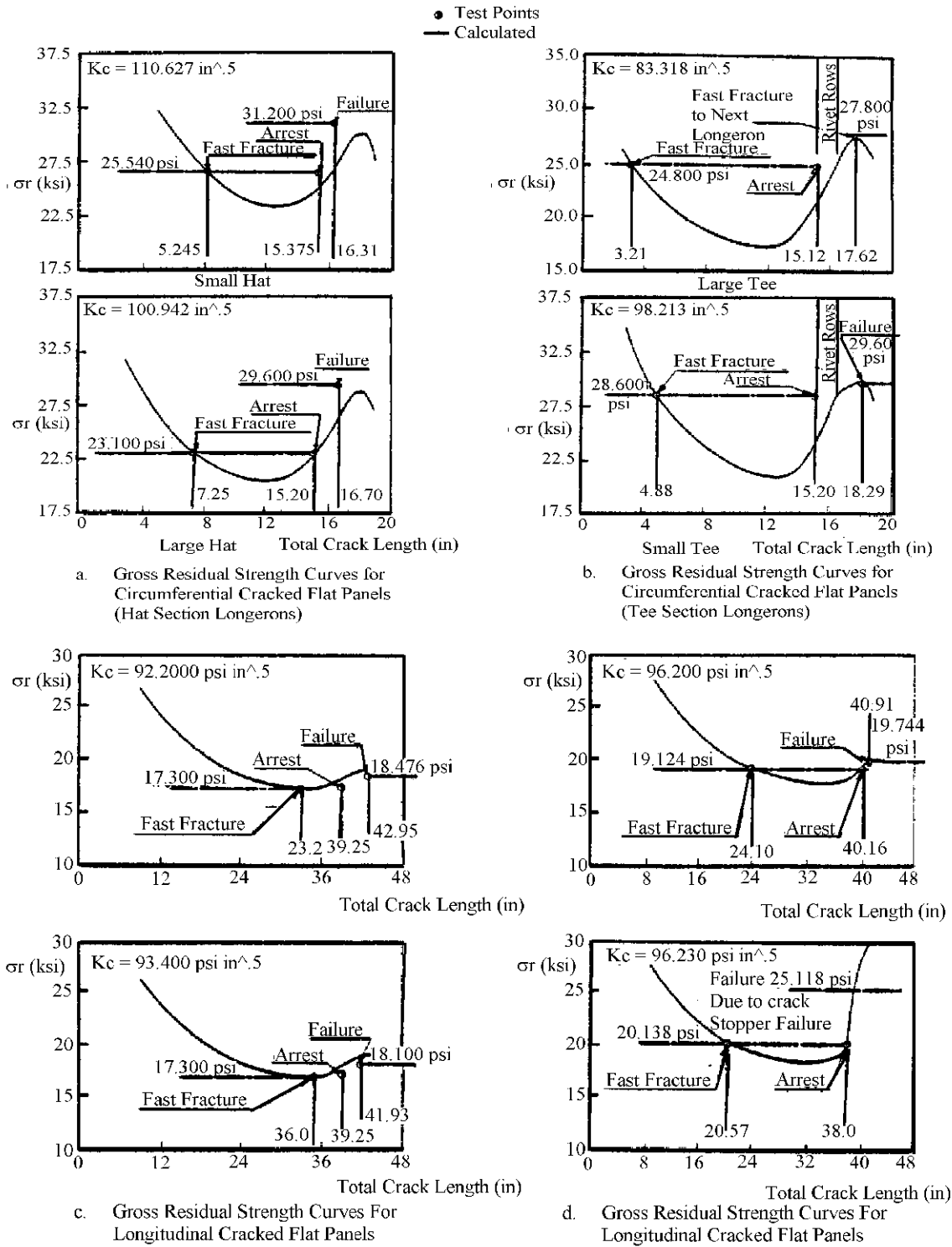


Figure 7.4.8. Test Results of Swift and Wang on 120 Inch Wide Panels with 7075-T73 Skin

A similar program was conducted by Dawicke, et al. [1999]. Under the auspices of the NASA Aircraft Structural Integrity (NASIP) and Airframe Airworthiness Assurance/Aging Aircraft (AAA/AA) programs, a residual strength prediction methodology has been experimentally verified for aircraft fuselage structures.

The fracture criteria selected for use on the (mostly) thin gage aluminum fuselage structure was the crack tip opening angle (CTOA). A detailed description of the testing methodology used for determining the COTA is given in Dawicke [1997] and Dawicke & Sutton [1993]. The COTA was selected to handle the diverse loading problems of large scale yielding, and significant stable crack growth which limited the applicability of more normal linear elastic fracture mechanics. Two finite element codes were used in the program: a) ZIP3D was used for the simple laboratory specimens which did not exhibit large out of plane displacements, b) STAGS, which is a nonlinear shell analysis code, was used for the residual strength analysis for larger specimens with large out of plane displacements.

A typical fuselage skin material, 2024-T3, was used throughout the program. Specimen thicknesses were 0.040, 0.063, and 0.090 inches. The laboratory test results of the CTOA were used to predict the results from larger structural element and full scale structure validation tests. The final test in the series was a full size fuselage segment with combined internal pressure loading and axial tension loads to simulate fuselage body bending.

The CTOA fracture criteria projects that crack growth will occur when the included angle of the two crack surfaces ([Figure 7.4.9](#)) with respect to the crack tip reaches a critical value. The critical angle for a given material is nearly constant after growth exceeds the half thickness point, as shown in [Figure 7.4.10](#). An increase in the thickness of the specimen causes a decrease in the CTOA, as shown in [Figure 7.4.11](#).

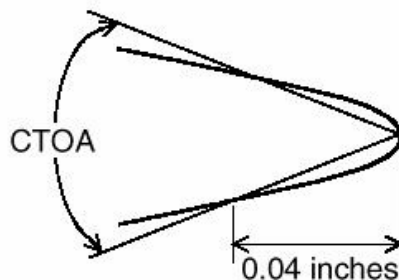


Figure 7.4.9. Schematic of the Definition of Critical Crack-Tip Opening Angle (CTOA)
[Dawicke, et al., 1999]

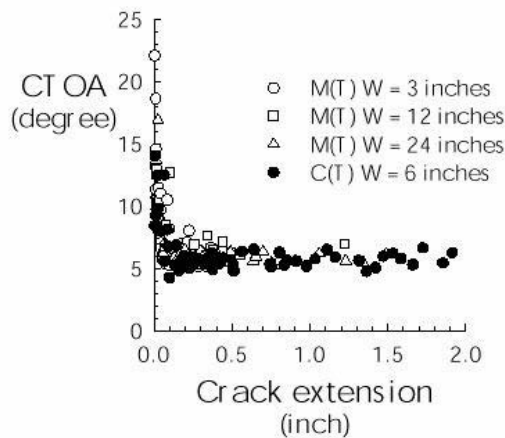


Figure 7.4.10. CTOA Measurements For 0.063-Inch-Thick, 2024-T3 Aluminum Alloy [Dawicke, et al., 1999]

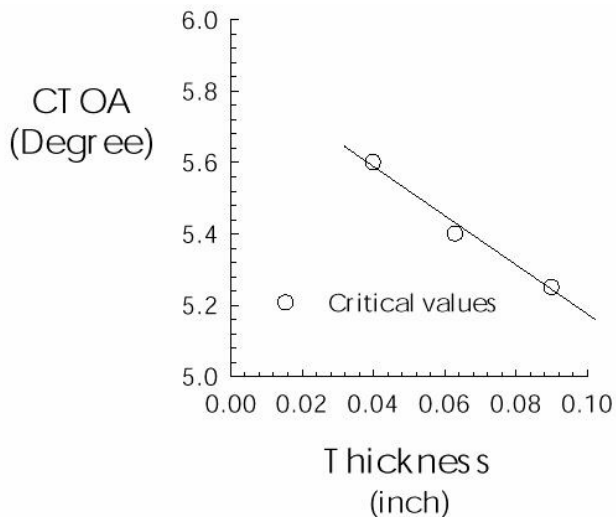


Figure 7.4.11. Influence Of Specimen Thickness On The Critical CTOA For 2024-T3 Aluminum Alloy [Dawicke, et al., 1999]

Another complexity that was introduced by using the STAGS 2D FEM was the necessity to account for the through-thickness constraint effects by using an approximation for the plane strain core (PSC). This approximation of the PSC height is nominally equal to or less than the specimen thickness ([Figures 7.4.12](#) and [7.4.13](#)).

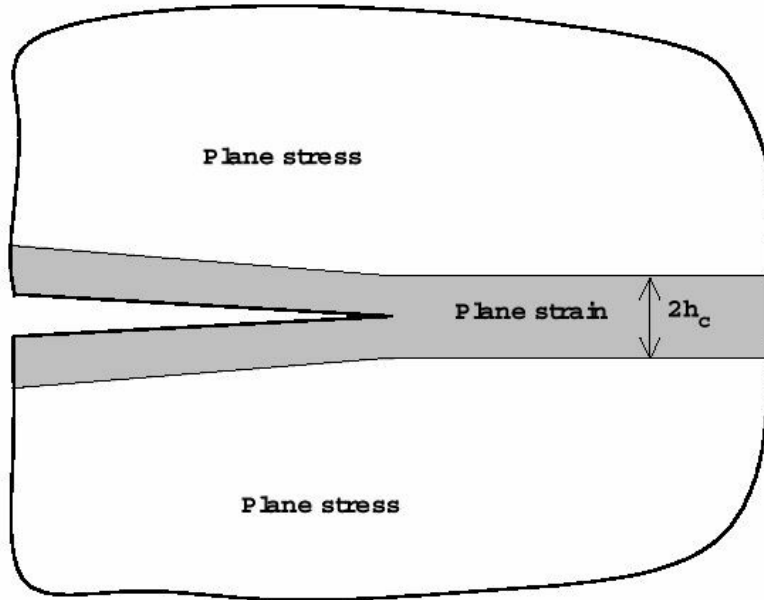


Figure 7.4.12. Illustration of the Plane Strain Core Around a Crack [Dawicke, et al., 1999]

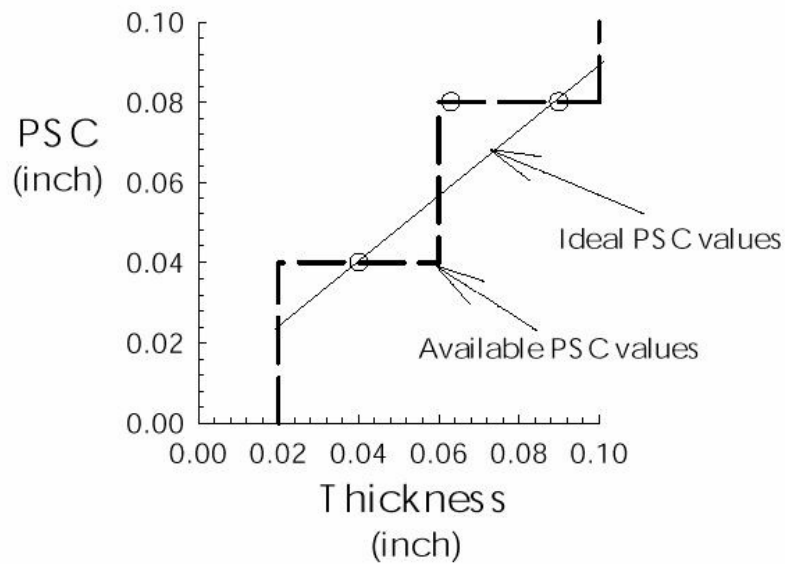


Figure 7.4.13. Plane Strain Core Heights (PSC) for the 0.04, 0.063, and 0.09-inch-thick 2024-T3 Aluminum Alloy Specimens [Dawicke, et al., 1999]

The report summarizes a successful application of the CTOA fracture criteria in conjunction with a 2D non-linear FEM model. The critical CTOA and the plane strain core (PSC) were acquired from small laboratory size specimens and the results were projected for wide panel (40 inches)

([Figure 7.4.14](#) and [7.4.15](#)) and full scale fuselage structural components. For a specified thickness, the predicted value to the experimental test value was within 10% for all the program specimens.

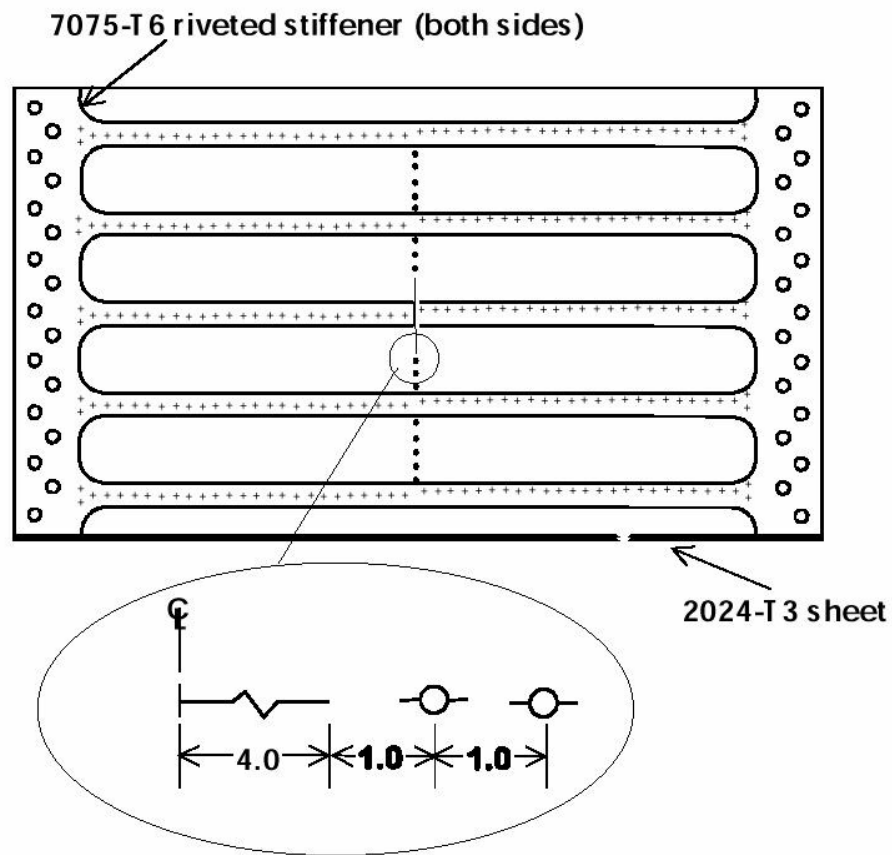


Figure 7.4.14. Stiffened Panel and MSD Crack Configuration [Dawicke, et al., 1999]

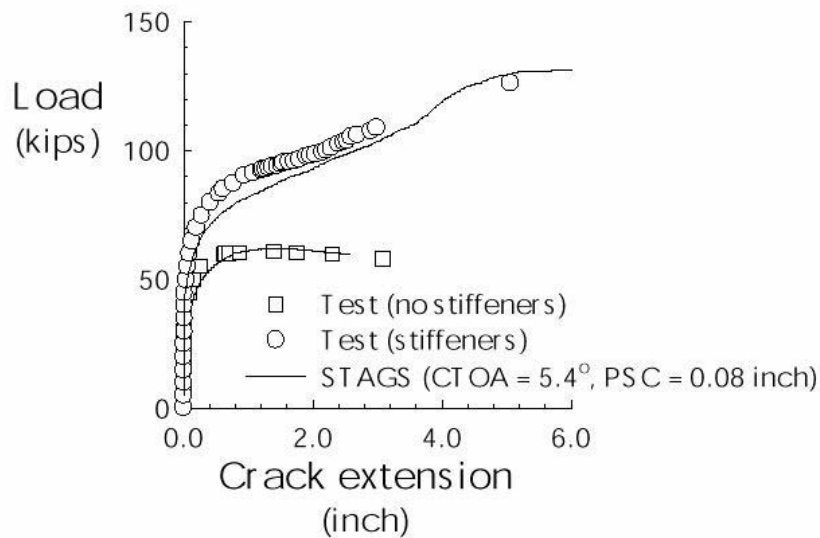


Figure 7.4.15. Fracture Test Results For 2024-T3, B=0.063-Inch-Thick, 40-Inch-Wide M(T) Specimens With and Without Stiffeners and STAGS Predictions Using CTOA=5.4° and PSC=0.08 Inch [Dawicke, et al., 1999]

The residual strength verification testing continues through both the design analysis and test development phase and the full-scale flight and ground test phase of an aircraft development contract (JSSG-2006 paragraph 4.12.2 and A4.12.2). For cost-effectiveness, it is useful to terminate a number of fatigue tests (used to verify the crack growth analysis or test spectrum design) with a controlled fracture test. Continuing a fatigue test until failure occurs may give incomplete or false information about the residual strength characteristics of the structure. Hence, it would not be appropriate to use fatigue failures to verify residual strength. The problems associated with attempting to verify residual strength analysis or characteristics using the information from fatigue test failures are summarized below:

- 1) The damage tolerance requirements specify residual strength loads, P_{xx} , which are all on the order of limit load. Stresses on the order of the limit load stress may occur seldom in the test stress history; they may not occur at all during the last part of crack growth. As a result, the cracks may grow much longer than the critical size associated with the stress level at the P_{xx} load. Then final failure will occur at a much lower stress.
- 2) Letting failure occur in the course of a crack growth test introduces a difficulty in determining the stress at fracture. If the loading is constant amplitude, it is reasonable to assume that fracture occurs at the peak stress. In variable-amplitude loading a series of low stress cycles may be followed by one high stress cycle during which fracture occurs. It is not certain now whether fracture took place at the peak or at a somewhat lower stress.
- 3) The critical crack size may be difficult to determine. Usually some crack growth has occurred since the last measurement. During the last cycles, crack growth

may accelerate fast. This usually means that the fracture surface is very similar to that of a static fracture. As a result, the size of the fatigue crack at which fracture occurred is not well delineated on the fracture surface.

- 4) The crack growth at low stresses may continue so long that fracture occurs at a crack size that is too long with respect to specimen dimensions. A rational comparison with other test data is complicated due to the remaining ligament requirements and could be misleading.

Therefore, it is useful to perform a controlled residual strength test near the end of the crack growth test. For this purpose, the critical crack size is estimated on the basis of the stress at the required P_{xx} . The test is discontinued when this crack size is reached. Then an appropriately instrumented fracture test is performed. In this respect, it is important that the specimen is of sufficient size. There can be no question about this when a complete component is tested. In that case, any size requirement is overruled.

7.4.3 Crack Growth Modeling-Verification

The basis of all crack growth calculations is the damage integration package discussed in Section 5, which includes the models and procedures used in estimating the effects of the load and environmental events in the operational history that must be verified. To model the impact that a variable amplitude load history has on the crack propagation characteristics of a structure, the damage integration package must be able to predict the effects of load amplitude, stress ratio (R), load sequences, and hold time events, as well as load frequency and waveshape in the case of a material sensitive to environmental effects.

Testing for verification of the crack growth models in the damage integration package should be conducted using middle-cracked panels. The middle-cracked panel geometry is characterized by widely accepted stress-intensity factor calibration and the results of spectrum tests with this geometry are easiest to correlate. It is recommended that the procedures outlined in Section 7.2 and in ASTM E647 relative to geometry, crack measurement, and pre-cracking be employed when using the middle-cracked panel specimen for non-constant amplitude loading.

Additional tests should be performed on specimens with radial corner cracked hole geometries and on specimens containing surface flaws in order to verify methods that describe the change in crack shape as the crack grows. It is important that corner-crack and surface-crack geometries be included in any crack growth verification test program in view of their relevance to the damage tolerance criteria. Radial corner-cracked-hole specimens and other part-through thickness specimens require special preparation techniques. Typically, the radial corner-cracked hole specimens are prepared in two steps. The first step is to introduce damage (EDM notch, saw cut, etc.) into a hole that is undersized and pre-crack the specimen until a crack of sufficient size appears. The second step is to enlarge the hole, remove the initial damage, and leave a crack with the required size in the specimen. It is necessary in the first step during pre-cracking to limit the stress-intensity factor levels so that the crack tip is not exposed to levels higher than what will be experienced during the test start up. Sometimes to preclude overload effects, the radial-cracked specimen is pre-cracked subsequent to the second step.

The surface flaw (part-through-crack) specimens are normally prepared along the lines suggested by ASTM E740. While the objective of this standard is to describe a fracture test of a part-

through-crack type structural geometry, the standard details damage preparation techniques as well as pre-cracking procedures.

Because each material responds differently to the same spectrum, and because each load history will cause different amounts of damage in different materials, a crack growth damage integration package will be based on a combination of models and experimentally established constants. Typically, the effects of load amplitude, stress ratio and load sequence are addressed through the use of a model that effectively combines a crack-growth-rate-based stress-ratio model with a crack-growth-retardation model which in turn accounts for the effect of tensile and compressive overloads, as well as multiple overload occurrences. The stress-ratio models as well as the retardation models are empirically based as was discussed in Section 5. The tailoring of the retardation model so that it adequately represents effects of a given spectrum and material is one of the more difficult tasks of the damage tolerant design analysis and test development activities.

The tailoring of the retardation model is based on crack growth life predictions of test results using reliable baseline (constant amplitude) crack growth rate data. In terms of developing a good correlation between prediction and test results, the following guidelines apply for each test. First and foremost, there should be a good estimate of the crack growth life based on the growth from crack initiation to test termination. Second, and normally just as important, the shapes of the predicted and test crack growth curves should match as closely as possible. [Figure 7.4.16](#) illustrates these two points: predictions A and B would be considered bad, even though the life to failure was predicted correctly. Correlations are considered good if the prediction of all relevant points are within about 20 percent of the test data, as indicated by the shaded region of the figure. Typically, a number of tests with different conditions must be conducted before the damage integration package can be accepted with confidence. It is recommended that each crack growth test be summarized with crack growth life curves (predicted and test). The next several paragraphs describe a verification test program for an improved damage integration package.

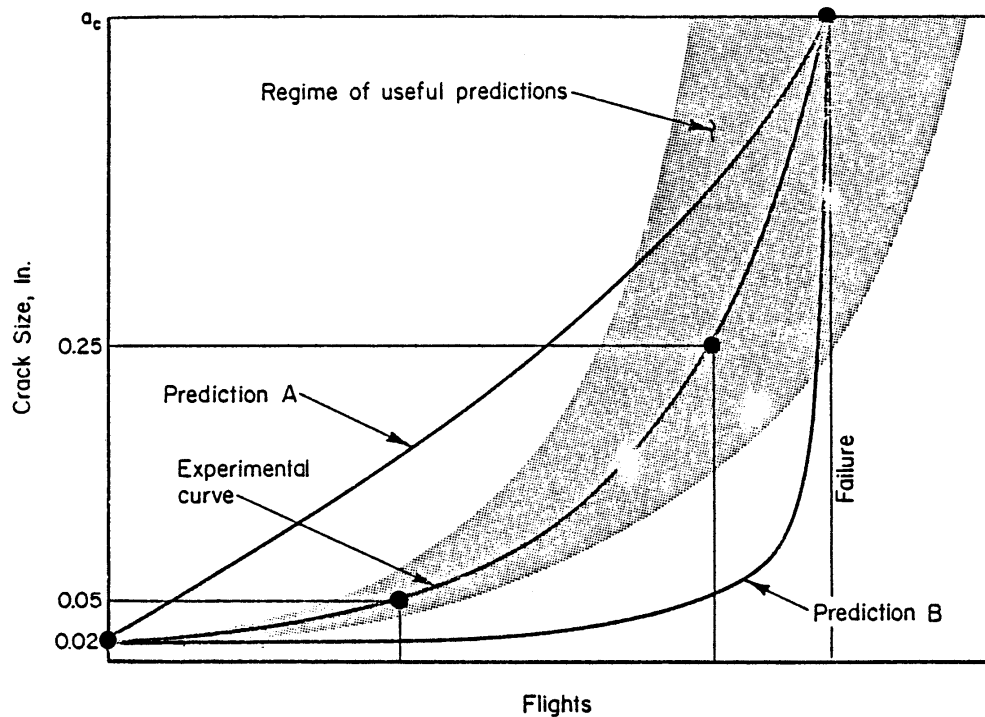


Figure 7.4.16. Comparison of Analytical and Experimental Crack Growth Curves

In a study for the (then) Flight Dynamics Laboratory, Chang [Chang, et al., 1978; Chang, et al., 1981; Chang, 1981] conducted a series of crack growth tests on 2219-T851 aluminum alloy that were used to verify the accuracy of an improved damage integration package imbedded within the computer code EFFGRO. In Chang, et al., [1981], Chang summarizes the results of ten constant amplitude tests (different stress ratios), 20 tests where single and periodic overloads were applied, and 30 tests where multiple overloads and block loading conditions were studied. In Chang [1981], Chang summarized thirteen tests where different flight-by-flight loading conditions were applied; eleven tests involved fighter histories, two tests involved transport type histories. [Table 7.4.3](#) summarizes the test program and Chang's ability to estimate the crack growth lives for the various types of test conditions based on the life prediction ratio approach.

The life prediction ratio (N_{pred}/N_{test}) is the life determined from the prediction divided by the life from the test and is calculated for each test. [Table 7.4.3](#) provides a collective summary of all the results that Chang developed, grouped in the same way that he presented the results as well as in larger groupings. For all the tests, the mean life prediction ratio is 0.987 and the standard deviation of this measure is 0.35; the lowest and highest life prediction ratios are 0.15 and 2.48, respectively. [Table 7.4.4](#) shows how the life prediction ratio statistics (mean and standard deviation) can be used to estimate the error in a crack growth life calculation based on the improved model. Note from [Table 7.4.4](#) that the damage integration package will predict lives that range between plus and minus (approximately) 60 percent of actual, 80 percent of the time.

Table 7.4.3. Summary of Chang’s Improved Spectrum Prediction Results Based on Tables in Chang, et al.[1981] and Chang [1981]

Chang’s Table No.	Number of Tests	Type of Load History	Life Prediction Ratios (N_{pred}/N_{test})		
			Mean \pm Standard Deviation	Lowest Value	Highest Value
2*	10	Constant amplitude	1.340 \pm 0.500	0.81	2.48
3*	19 ⁺	Single and periodic overload	0.783 \pm 0.240	0.37	1.18
4*	30	Multiple overload and block	0.938 \pm 0.30	0.15	1.60
2* and 3*	29	See above	0.974 \pm 0.44	0.37	2.48
2*, 3* and 4*	59	All simple	0.956 \pm 0.37	0.15	2.48
2 ⁺⁺	13	Flight-by-flight	1.131 \pm 0.22	0.80	1.46
2*,3*,4* and 2 ⁺⁺	72	All	0.987 \pm 0.35	0.15	2.48

+ one additional test reported but life estimate vague

* from Chang, et al. [1981]

++ from Chang [1981]

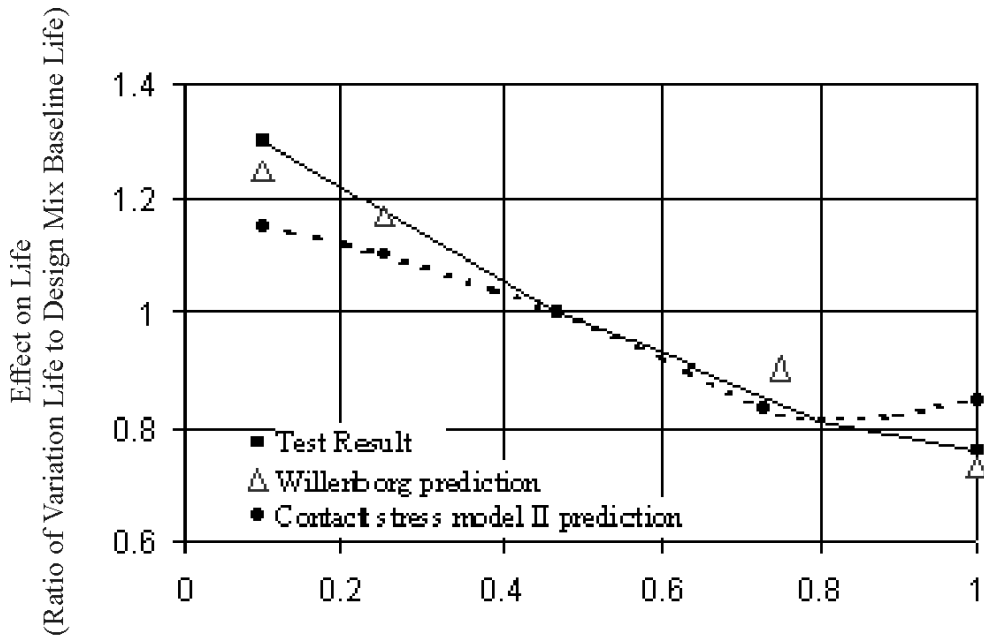
Table 7.4.4. Error Estimate in Life Prediction Ratio Based on Assumed Normal Distribution of All Chang’s Results (72 Tests)

Probability of Maximum Error Occurring (%)	Formula For Estimating Errors	Life Prediction Data For Estimating Errors (See Table 7.4.2)	Lowest Error Expected (N_{pred}/N_{test})	Highest Error Expected (N_{pred}/N_{test})
± 1	Mean \pm 2.58 Std. Dev.	0.987 \pm 2.58 \times 0.35	0.084	1.89
± 5	Mean \pm 1.96 Std. Dev.	0.987 \pm 1.96 \times 0.35	0.301	1.67
± 10	Mean \pm 1.645 Std. Dev.	0.987 \pm 1.645 \times 0.35	0.411	1.56

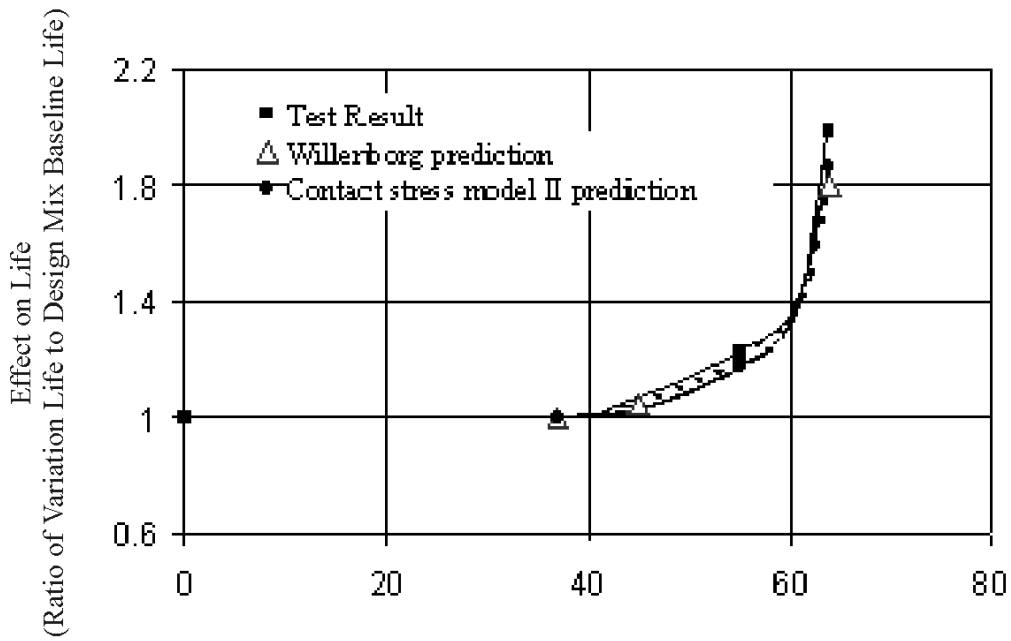
By collectively evaluating the life prediction ratios for the individual tests, for selective test groupings, and for the total number of tests conducted, the engineer can evaluate both the effectiveness of the modeling approach as well as the accuracy of individual tests. Improvements in the more fundamental segments of the model might yield substantial improvements in all the life prediction ratios, whereas isolated modification of some empirical constants might only improve the predictability of a limited number of tests. It is recommended that life prediction ratio data such as illustrated in [Table 7.4.3](#) provide the basis for justifying selection of damage integration packages. In fact, by using such schemes for different crack geometries or load transfer situations, the engineer will have the necessary confidence that crack

growth life predictions for more complicated cases can be made with the best possible reliability. See Saff & Rosenfeld [1982], Wozumi, et al. [1980], Rudd, et al. [1982], Dill, et al. [1980], Abelkis [1980] and Lambert & Bryan [1978] for other examples of test programs designed to verify the capability of a damage integration package.

In the design of a given airplane component, generality is not required if the damage integration package applies well to the spectrum and history of that component. The most applicable prediction method has to be found. The only basis for judgment of the applicability is a series of tests with the relevant spectrum and stress history. Therefore, it is recommended that some substantiation testing be performed as soon as there is reasonable certainty with respect to the spectrum shape. The experiments should be performed on a flight-by-flight basis, with landing loads included. A reasonable number of stress levels should be used as discussed in Section 5.3. The stress sequence within a flight should be representative for service usage (Section 5) or arranged in a lo-hi-lo sequence. Block loading should not generally be applied. Experiments should be run for a few different design stress levels and one or two clipping and truncation levels in order to evaluate the effect of these changes on crack growth behavior, and to justify proposed changes to the design spectrum for component and full-scale fatigue testing. [Figure 7.4.17](#) describes the results of one comparative study [Dill, et al., 1980].



(a) Effect of Mission Mix on Crack Growth Life



(b) Truncation Level
(Percent Limit Stress Level Below Which Loads are Truncated)

Figure 7.4.17. Effect of Spectrum Variations on Crack Growth Life Compared to Baseline (Design Mix) and to Two Damage Integration Packages [Dill, et al., 1980]